Lasers in Manufacturing Conference 2021

Influence of laser focus shift on porosity and surface quality of additively manufactured Ti-6Al-4V

Nicole Emminghaus[a,*], Christian Hoff[a], Jörg Hermsdorf[a], Stefan Kaierle[a]

[a]*Laser Zentrum Hannover e.V., Hollerithallee 8, 30419 Hannover, Germany*

Abstract

In laser-based powder bed fusion of metals (PBF-LB/M) an increase of the laser spot size by shifting the focus position (defocusing) offers the opportunity of reducing the overall scanning time as well as achieving a more stable melt pool behavior. However, the influence on porosity and surface roughness of bulk samples has received little attention so far. In this work, the influence of laser defocusing (Yb-fiber laser, minimum beam diameter of 35 µm) on part porosity as well as top and side surface roughness is investigated for additively manufactured Ti-6Al-4V. Therefore, the focusing lens position relative to its standard setting is investigated in a range between 1.2 mm and -8.7 mm. Additionally, the main processing parameters are varied and their influences and interaction effects are statistically evaluated according to the design of experiments approach. Optimum settings for low porosity and surface roughness are presented.

Keywords: Laser powder bed fusion; additive manufacturing; Ti-6Al-4V; defocusing; porosity; surface quality

1. Introduction

Laser-based Powder Bed Fusion of Metals (PBF-LB/M), also known as Selective Laser Melting (SLM®), is an Additive Manufacturing (AM) technology for processing metal powders in a layerwise manner. Thereby the source of energy to melt the powder is a laser, usually a fiber laser that provides a high beam quality. The 3D model of the part is first created using a CAD (computer-aided design) software and then sliced with a typical layer thickness of 20 µm - 100 µm. This manufacturing technique allows the realization of complex geometries and features like internal cooling channels or lattice structures that could not be built with conventional processing techniques. Additionally, the cost per part remains the same regardless of its complexity. However,

* Corresponding author. Tel.: +49-511-2788-355; fax: +49-511-2788-100 .
E-mail address: n.emminghaus@lzh.de

build rates and therefore the productivity are quite low in comparison with other manufacturing techniques, e.g. DED (Direct Energy Deposition) (Metelkova et al., 2018). A higher build rate can most effectively be achieved by an increase of layer thickness and laser power, leading to a constant volume energy density, but at the cost of decreasing geometrical resolution (Schleifenbaum et al., 2010).

According to (Ciurana et al., 2013; Gunenthiram et al., 2018; Metelkova et al., 2018) the volume energy density E_V can be given as

$$E_V = \frac{P}{v \cdot d_{spot} \cdot t} \qquad (1)$$

with the laser power P, the scanning speed v, the laser spot diameter d_{spot} and the layer thickness t.

According to this equation, another parameter that can be varied to adjust the build rate by adjusting the energy density is the spot diameter. For example, the study of Metelkova et al. showed that an 840 % increase in productivity is possible by implementing laser defocusing (Metelkova et al., 2018). A larger spot allows the increase of the hatch spacing and therefore reduced layer scanning times. Further, an enlarged beam diameter can reduce the amount of spattering when increasing the applied laser power (Schleifenbaum et al., 2010). The simplest way to adjust the spot diameter in the working plane is to defocus the laser beam. Beam defocusing and its effects on part properties recently attracted growing interest and was investigated by several research groups and for different materials.

Soylemez used a defocused laser beam and investigated different parameter settings to avoid pore generation due to keyholing and to increase the deposition rate of Ti-6Al-4V single bead meltpool geometries (Soylemez, 2020).

Shi et al. processed single lines and bulk Ti-6Al-4V specimens using different beam diameters (50 µm and 200 µm) und demonstrated that a larger beam diameter could enhance process stability and reduce defect generation. They concluded that a larger beam diameter is more suitable for processing with higher laser power and layer thickness (Shi et al., 2018).

McLouth et al. found that the microstructure of Inconel 718 significantly depends on the applied focus shift and the resulting beam diameter and energy density. They thus proposed to use this for microstructure tailoring (McLouth et al., 2018).

Metelkova et al. implemented different defocus distances with both positive and negative signs for the processing of 316L. For the same settings of laser power and scanning speed the melt pool width and depth were significantly larger if the defocus distance had a negative sign (focus situated below the working plane)(Metelkova et al., 2018).

Zhou et al. used defocusing amounts between -2 mm and 2 mm and found that this parameter strongly affects the melt pool structure as well as the relative density and the resulting mechanical properties of AlSi10Mg. They also observed a dependence on the defocusing sign with a larger penetration depth for negative signs (Zhou et al., 2019).

Similar results were also obtained by Nie et al. for a high strength Al–Cu–Mg–Mn alloy, who varied the defocus in a range between -3 mm and 3 mm. They observed a keyhole or transition mode melting for negative signs and conduction mode melting for positive signs resulting in different amounts of pores and cracks (Nie et al., 2020).

The given literature review demonstrates that laser beam defocusing can be used to increase the process productivity as well as to adjust the parts properties like microstructure and amount of defects based on the present melting mode. However, the amount of studies is still relatively small especially regarding individual materials like Ti-6Al-4V, which is of high industrial relevance. In addition to that, the effect of laser defocusing on part quality and its correlation with relative density and as-built surface roughness was not sufficiently

investigated yet. Therefore, this work focusses on the effect of laser defocusing on the relative density, the resulting surface quality as well as the interaction effects of defocusing and the main parameters laser power and scanning speed as well as layer height.

2. Materials and Methods

2.1. Experimental Materials

In this work, gas atomized Ti-6Al-4V grade 23 powder supplied by Heraeus Additive Manufacturing GmbH was used. The size distribution of the virgin powder exhibits the percentiles (D-values) 22 µm (D10), 38 µm (D50) and 54 µm (D90), according to the manufacturer's data sheet. Reuse and recycling of powder is of growing interest for industrial applications with regard to resource efficiency and cost reduction. Therefore, the powder used in this work was already recycled multiple times before. An exact number of reusing cycles cannot be given, because the powder circulates permanently in the used machine. The powder was analyzed using scanning electron microscopy (SEM, Quanta 400 FEG, FEI Company). As it can be seen in Fig. 1, the powder particles are mainly spherical.

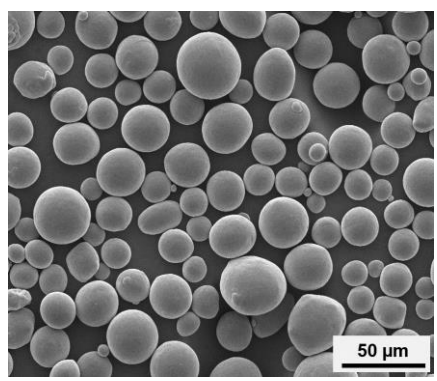

Fig. 1. SEM image of Ti-6Al-4V powder.

2.2. Experimental Equipment

The experiments were carried out on the industrial machine Lasertec 12 SLM by DMG MORI ADDITIVE GmbH (Bielefeld, Germany), that is equipped with a 400 W ytterbium fiber laser (single mode, continuous wave, wavelength 1070 nm). It supplies a high quality laser beam (M^2 = 1.05) with a minimum spot diameter of 35 µm. The z-position of the spot can be shifted by variation of the position of the integrated focusing lens, called lens position. This way it is possible to change the spot diameter in the working plane. Argon was used as shielding gas to prevent oxidation. Thereby, a minimum residual oxygen content of 1000 ppm can be achieved in the machine.

2.3. Experimental Methods

To examine the influence of the variation of the focusing lens position, two separate experimental runs were conducted.

Within the first run, the standard processing parameters laser powder *P*, scanning speed *v* and hatch spacing *h* as well as the layer thickness *t* were kept constant with settings that were chosen according to the machine manufacturers recommendations. The only varied parameter in this run was the lens position. Table 1 gives an overview of the parameters implemented for the first run. Contour and infill were processed with different parameters. Thereby, the contour was scanned after the infill. For each lens position, three specimens were built.

Table 1. Levels of the varied processing parameters in the first experimental run.

Parameter	**Levels**	
Lens position (mm)	-8.7, -8.4, -7.8, -7.2, -6.6, -6.0, -5.4, -4.8, -4.2, -3.6, -3.0, -2.4, -1.8, -1.2, -0.6, 0.0, 0.6, 1.2	
Layer thickness (µm)	30	
Hatch spacing (µm)	80	
	Infill	**Contour**
Laser power (W)	175	120
Scanning speed (mm/s)	1050	860

For the second experimental run, a circumscribed central composite design was implemented. This design allows the estimation of first- and second-order terms, including two-factor interaction effects. Therein, the varied factors were the laser power and the scanning speed, due to their superior influence on the part quality compared to the hatch spacing, as well as the lens position. Here, the range of the values for the lens position were chosen based on the results of the first run. To additionally investigate the influence of the lens position with regard to the build rate, the layer thickness was varied in three levels. The chosen parameter values for all levels are shown in Table 2. The same parameters were used for the contour and the infill in this run to reduce the number of possible influencing factors. The hatch spacing was again kept constant at 80 µm.

Table 2. Levels of the varied processing parameters in second experimental run according to the central composite design.

Parameter	**Levels**				
Laser power (W)	150	175	200	225	250
Scanning speed (mm/s)	600	800	1000	1200	1400
Lens position (mm)	-6	-4.5	-3	-1.5	0
Layer thickness (µm)	30		60		90
Hatch spacing (µm)			80		

For generation, evaluation and analysis of the experimental design and data, the statistics software JMP® (SAS Institute Inc.) was used. A significance level of 5 % was chosen. All not significant terms (p-value > 0.05) were excluded under the condition that there were no significant dependent higher order effects following the principle of strong effect heredity. The mathematical model was fitted using the least squares method.

The specimens were built with a cubic shape, a side length of 5 mm and on top of 3 mm support structures. A cross-hatching strategy with a rotation angle of 67 ° between adjacent layers was applied. The specimens were placed randomly on the build platform to exclude the influence of the position determined by direction

of gas flow and coater movement. The platform was preheated to 100 °C to reduce thermal stresses and the minimum residual oxygen content of 1000 ppm was maintained throughout the process.

2.4. Methods for Analysis

After manual removal from the build platform, the top (horizontal) and side (vertical) surface of the cubic specimens were analyzed by optical profilometry (OP) using the Keyence laser scanning confocal microscope VK-X1000. The arithmetic mean roughness (S_a) was calculated as the quantitative roughness measurement for a quadratic area with a side length of 2000 µm. S_a is one of many roughness metrics that is used in literature to describe roughness of AM parts (Grimm et al., 2015). Its linear corollary is R_a. S_a is defined as the average of roughness height of each point relative to the arithmetical mean of the surface.

After surface characterization, all samples were cold embedded in epoxy resin (Technovit Epox, Kulzer GmbH, Hanau, Germany), ground and polished (Tegramin, Struers ApS, Ballerup, Denmark). Three cross-sections were made parallel to the build direction (BD) for every sample. The metallographic cross-sections were analyzed using light microscopy. The single images were stitched and subsequently analyzed using a python script developed at Laser Zentrum Hannover e. V. (LZH). This script includes the image transformation to black and white with a given threshold value and a subsequent calculation of the relative density (ratio of black and white pixels). Finally, the mean relative density of all three cross-section was calculated for each sample.

3. Results and Discussion

In the first experimental run, the only varied parameter was the lens position. As it can be seen in Fig. 2, a strong dependence of surface roughness, especially the top surface roughness, as well as the relative density could be observed. For the relative density a maximum value of 99.99 % (lens position: -3 mm) and a minimum value of 89.40 % (lens position: -8.4 mm) were obtained. While the relative density is constantly above 99.00 % for a lens position between -6.0 mm and 1.2 mm it strongly decreases for increasing negative values of the lens position. Additionally, it can be seen that with increasing negative lens position, the density variation between samples build with the same parameters increases. The top surface roughness increases as the relative density decreases. For the side surface roughness, no dependence on the relative density can be seen.

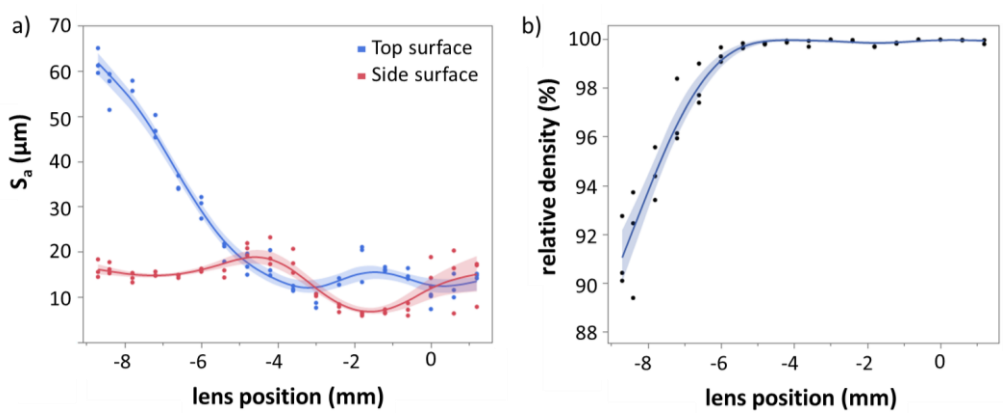

Fig. 2. a) Surface roughness S_a in dependence of lens position, b) relative density in dependence of lens position; cubic spline with lambda = 0.05 used as smoother in both graphs, shaded areas represent the confidence intervals.

A minimum side surface roughness of 5.893 µm could be obtained for a lens position of -1.8 mm and a maximum value of 23.218 µm was reached at a lens position of -4.2 mm. The minimum top surface roughness was 7.351 µm (lens position: 0.0 mm), the maximum was 65.046 µm (lens position: -8.7 mm) and thus significantly (2.8 times) larger than the maximum side surface roughness.

These observations show that there is a correlation between relative density and the top surface roughness and both, relative density and roughness, are negatively influenced by the lens position, if values below -6.0 mm are implemented. It is assumed that for values closer to 0.0 mm (focal plane is in working plane) the volume energy density, given in equation (1), stays in a range that is sufficient to fully melt the powder. Consequently, a smoother surface and less defects can be obtained. When the distance between focal plan and working plane exceeds a critical value, the energy input is insufficient to melt the powder and fuse the single layers resulting in rough surfaces with open porosity as well as lack of fusion pores.

Based on the results of the first run, the values for the lens position of the second run where chosen to be between -6.0 mm and 0.0 mm to stay in the range of values that lead to acceptable surface roughness and relative density, below 20 µm and above 99 %, respectively. For the second run the effects and interactions between the lens position and the other processing parameters were evaluated with regard to the surface roughness and relative density. For each of the three target sizes a model was fitted. Table 3, 4 and 5 display the estimates of the models coefficients, their standard errors and t-ratios (estimate divided by the standard error) as well as the according p-value. The effects and interactions will be described and discussed in the following.

3.1. Top surface roughness

The top surface roughness was most affected by the lens position whereby both the linear and the quadratic effect were found to be significant according to their p-values. The second most influential parameter was the layer height followed by the laser power. Additionally, there were significant interaction effects between different parameters with the interaction of laser power and lens position as the strongest one (Table 3).

Table 3. Parameter estimates for top surface roughness in descending order with corresponding standard error, t-ratio and p-value.

Term	Estimate	Std. Error	t-Ratio	p-Value
Intercept	16.38	15.81	1.04	0.3084
lens position	-2.25	$5.55*10^{-1}$	-4.06	0.0003
lens position²	1.79	$4.44*10^{-1}$	4.03	0.0003
layer height	$3.62*10^{-1}$	$3.51*10^{-2}$	10.33	0.0001
laser power	$-2.25*10^{-1}$	$6.47*10^{-2}$	-3.48	0.0015
laser power*lens position	$8.70*10^{-2}$	$3.14*10^{-2}$	2.77	0.0093
scanning speed	$1.10*10^{-2}$	$8.09*10^{-3}$	1.36	0.1835
scanning speed*lens position	$-9.06*10^{-3}$	$3.92*10^{-3}$	-2.31	0.0277
layer heigth²	$4.39*10^{-3}$	$2.03*10^{-3}$	2.17	0.0380
scanning speed*layer height	$-5.60*10^{-4}$	$1.70*10^{-4}$	-3.30	0.0025
laser power*laser power	$-1.17*10^{-4}$	$1.60*10^{-3}$	-0.07	0.9423
laser power³	$9.11*10^{-5}$	$3.55*10^{-5}$	2.57	0.0153
scanning speed²	$6.64*10^{-5}$	$2.50*10^{-5}$	2.66	0.0124
scanning speed³	$-1.48*10^{-7}$	$6.93*10^{-8}$	-2.14	0.0406

In Fig. 3 the response surface based on the parameter estimates is shown exemplarily for the three most influential parameters, i.e. the interaction of laser power and lens position as well as laser power and layer height. While for a lens position of 0.0 mm the top surface roughness increases for increasing laser power it decreases when a large negative value for the lens position is implemented. This can be explained by the

energy density that decreases with increasing distance between focal plane and working plane, so with a larger spot diameter, and also with decreasing laser power. Consequently, for large values of the lens position, a high laser power is needed to still sufficiently melt the powder. Additionally, with an increasing laser power and thus increasing melt temperature the viscosity of the melt decreases, so it can spread more easily and form a smooth, flat surface (Khorasani et al., 2020; Pal et al., 2020). According to equation (1), the scanning speed also influences the energy density and the statistical analysis showed a significant influence of this parameter. With increasing scanning speed, the energy density decreases und top surface roughness increases.

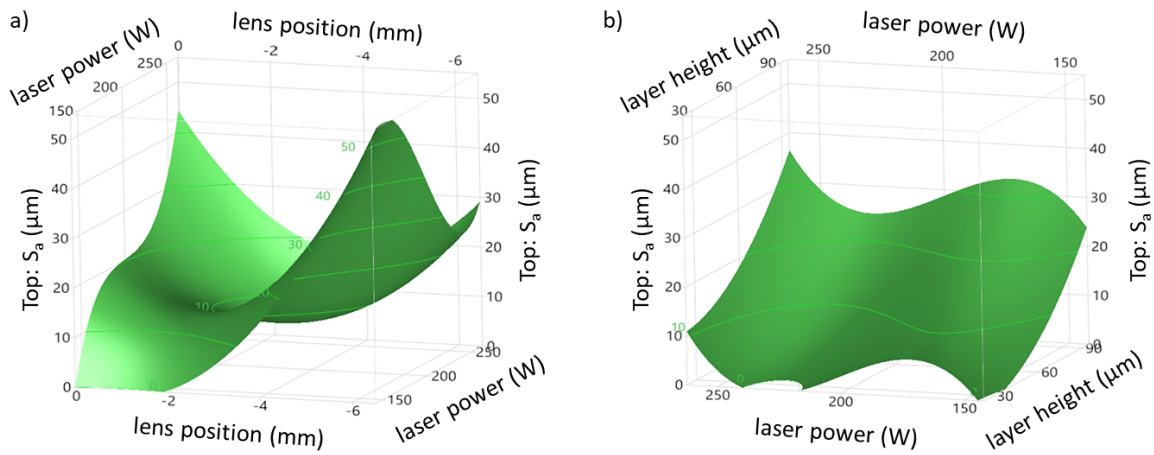

Fig. 3. Response surface plots of the top surface roughness: a) in dependence of laser power and lens position, b) in dependence of laser power and layer height.

For a minimum top surface roughness, a minimum layer height (30 µm), a high laser power of around 230 W, a medium scanning speed around 830 mm/s and a lens position of -3.6 mm are required according to the fitted model.

3.2. Side surface roughness

In contrast to the top surface roughness, the side surface roughness only depends significantly on lens position and layer height. Thereby, the influence of the lens position, i.e. its linear, quadratic and cubic effect, is stronger than the linear effect of the layer height. The estimates are shown in Table 4. Further, no significant interactions could be observed for this target size. Fig. 4 displays the response surface in dependence of the two significant factors. A minimum side surface roughness can be obtained for a lens position of -1.55 mm, according to the mathematical model. For increasing as well as decreasing values for the lens position from this point the side surface roughness also increases. It also in general increases for increasing layer height.

Table 4. Parameter estimates for side surface roughness in descending order with corresponding standard error, t-ratio and p-value.

Term	Estimate	Std. Error	t-Ratio	p-Value
Intercept	-9.04	2.14	-4.22	0.0001
lens position	-6.21	$5.74*10^{-1}$	-10.83	<0.0001
lens position²	1.13	$1.64*10^{-1}$	6.88	<0.0001
lens position³	$4.68*10^{-1}$	$8.75*10^{-2}$	5.34	<0.0001
layer height	$6.64*10^{-2}$	$1.87*10^{-2}$	3.56	0.0010

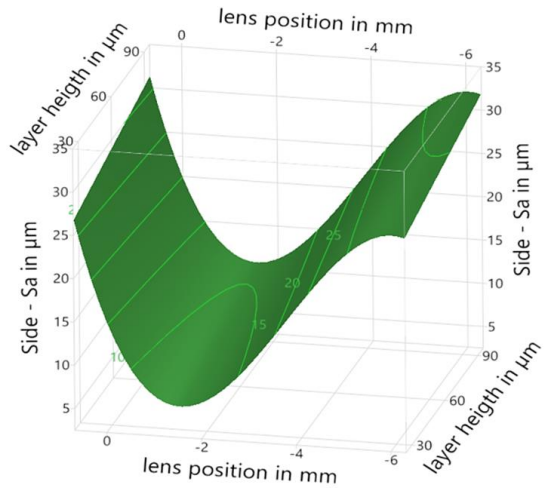

Fig. 4. Response surface plot of the side surface roughness in dependence of layer height and lens position.

These observations can be attributed to the layerwise build up leading to the stair-step effect, powder particles sintered to the side surface in each of these molten layers as well as open porosity due to insufficiently molten areas (Li et al., 2016). The strong decrease of the roughness when moving toward a lens position of zero can be attributed to a change in melting mode. As described in other studies (Zhou et al., 2019; Nie et al., 2020) a smaller spot size and therefore higher energy density as well as the convergent nature of the laser beam when using negative defocusing (Metelkova et al., 2018) promotes evaporation, keyholing and melt pool instabilities. Consequently, a higher surface roughness is generated. According to the described model, a minimum side surface roughness can be achieved by implementing a minimum layer height (30 µm) together with a lens position of -1.55 mm.

3.3. Relative densityTable 5 gives an overview on the effects that were found to be significant for the relative density. The lens position (linear and quadratic effect) had the strongest influence, followed by the layer height. The strongest interaction was found to be between layer height and lens position followed by the one of laser power and lens position. The response surface plots displaying these interactions can be seen in Fig. 5. The larger the negative value of the lens position is the higher is the laser power that is needed to process parts with high relative density. As before for the top surface roughness, this can be explained with the relationship between laser power, focus position and energy density. With increasing spot size due to increasing distance between focal plane and working plane the energy density (equation (1)) decreases, while it increases with increasing laser power. A similar explanation can be given for the observed

interaction between lens position and layer height. The value of the lens position for which a maximum relative density can be obtained moves toward zero for increasing layer height. This is because for thicker layers a higher amount of energy is needed to melt the powder and sufficiently fuse the adjacent layers.

From this, it is deduced that to increase the build rate by increasing the layer thickness the lens position should be carefully adjusted based on the layer height. Additionally, a lack of energy input due to defocusing could partly be compensated by increasing the laser power, e.g. when implementing a lens position of -6.0 to achieve a large spot, the density can be increased by around 4 percentage points when increasing the laser power from 140 W to 240 W.

In the case of a strongly defocused beam (lens position of -6.0 mm) a minimum layer height (30 µm), a high laser power of 250 W and a medium scanning speed around 910 mm/s are required for maximum density based on the presented model. In contrast, when working without defocusing (lens position of 0.0 mm) a larger layer height of 90 µm, a lower laser power of around 150 W and a high scanning speed of 1400 mm/s are suggested for maximum relative density.

Table 5. Parameter estimates for top surface roughness in descending order with corresponding standard error, t-ratio and p-value.

Term	Estimate	Std. Error	t-Ratio	p-Value
Intercept	102.33	1.43	71.68	<0.0001
lens position	$1.89*10^{-1}$	$7.25*10^{-2}$	2.61	0.0138
lens position²	$-9.33*10^{-2}$	$4.39*10^{-2}$	-2.12	0.0416
layer height	$-1.39*10^{-2}$	$4.58*10^{-3}$	-3.04	0.0047
layer height*lens position	$1.04*10^{-2}$	$2.96*10^{-3}$	3.50	0.0014
laser power*lens position	$-9.66*10^{-3}$	$4.10*10^{-3}$	-2.36	0.0247
laser power	$4.81*10^{-3}$	$4.35*10^{-3}$	1.11	0.2770
scanning speed	$-2.05*10^{-3}$	$1.06*10^{-3}$	-1.94	0.0616
scanning speed*lens position	$1.85*10^{-3}$	$5.12*10^{-4}$	3.61	0.0010
scanning speed*layer height	$-4.97*10^{-5}$	$2.22*10^{-5}$	-2.24	0.0322
scanning speed*layer height*lens position	$4.31*10^{-5}$	$2.09*10^{-5}$	2.06	0.0473
scanning speed²	$-9.77*10^{-6}$	$2.47*10^{-6}$	-3.95	0.0004
scanning speed³	$3.68*10^{-8}$	$9.06*10^{-8}$	4.07	0.0003

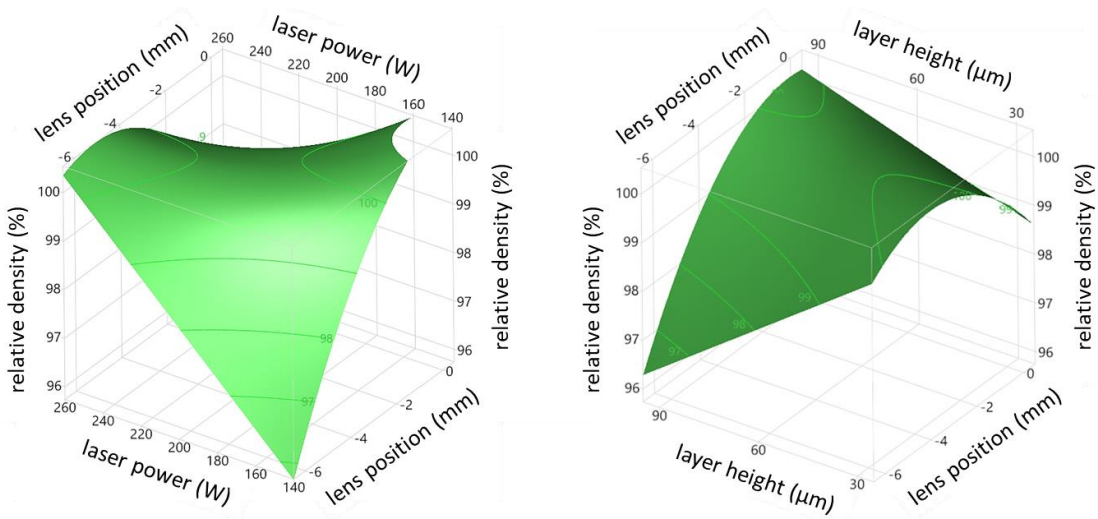

Fig.5. Response surface plots of the top surface roughness: a) in dependence of laser power and lens position, b) in dependence of lens position and layer height.

4. Conclusions

In this work, the effect of laser defocusing on the relative density, the resulting surface quality as well as the interaction effects of defocusing and the main process parameters were investigated. The estimates as well as response surface plots of the fitted mathematical models were presented. It could be demonstrated that the focusing lens position significantly influences the roughness on the top as well as on the side surface. Additionally, it is the most influential factor of the ones investigated in this study regarding the relative density.

The following conclusions can be drawn:

- Top surface roughness as well as relative density show a strong correlation and both depend on the volume energy density that is influenced by the defocusing by adjustment of the lens position, the laser power and the layer height.
- The side surface roughness is significantly affected by defocusing as well as the implemented layer high. An increase of layer height leads to an increase of side surface roughness. The amount of defocusing needs to be adjusted for the specific side surface roughness requirements.
- Defocusing should be compensated by a high laser power to achieve low top surface roughness and high relative density. For a high defocusing amount, by increasing the laser power by 100 W, the density can be increased by up to 4 percentage points. Additionally, increasing the build rate by increasing the layer thickness should be accompanied by an increase of laser power and a carefully adjusted lens position.
- The optimum settings for maximizing the relative density and minimizing surface roughness are different. A compromise between surface quality, density and build rate needs to be made.
- In future research the investigations should be supplemented by process monitoring to gain additional insights into the melt behavior.

References

Ciurana, J., Hernandez, L., Delgado, J., 2013. Energy density analysis on single tracks formed by selective laser melting with CoCrMo powder material. The International Journal of Advanced Manufacturing Technology 68(5-8), p. 1103-1110.

Grimm, T., Wiora, G., Witt, G., 2015. Characterization of Typical Surface Effects in Additive Manufacturing With Confocal Microscopy. Surf. Topogr. Metrol. Prop. 3(1), 014001.

Gunenthiram, V., Peyre, P., Schneider, M., Dal, M., Coste, F., Koutiri, I., Fabbro, R., 2018. Experimental analysis of spatter generation and melt-pool behavior during the powder bed laser beam melting process. Journal of Materials Processing Technology 251, p. 376-386.

Khorasani, M., Ghasemi, A., Awan, U. S., Hadavi, E., Leary, M., Brandt, M., Littlefair, G., O'Neil, W., Gibson, I., 2020. A study on surface morphology and tension in laser powder bed fusion of Ti-6Al-4V. The International Journal of Advanced Manufacturing Technology 111(9), p. 2891-2909.

Li, P., Warner, D. H., Fatemi, A., Phan, N., 2016. Critical assessment of the fatigue performance of additively manufactured Ti-6Al-4V and perspective for future research. International Journal of Fatigue 85, p. 130-143.

McLouth, T. D., Bean, G. E., Witkin, D. B., Sitzman, S. D., Adams, P. M., Patel, D. N., Park, W., Yang, J.-M., Zaldivar, R. J., 2018. The effect of laser focus shift on microstructural variation of Inconel 718 produced by selective laser melting. Materials & Design 149, p. 205-213.

Metelkova, J., Kinds, Y., Kempen, K., de Formanoir, C., Witvrouw, A., & Van Hooreweder, B., 2018. On the influence of laser defocusing in Selective Laser Melting of 316L. Additive Manufacturing 23, p. 161-169.

Nie, X., Chen, Z., Qi, Y., Zhang, H., Zhang, C., Xiao, Z., Zhu, H., 2020. Effect of defocusing distance on laser powder bed fusion of high strength Al–Cu–Mg–Mn alloy. Virtual and Physical Prototyping 15(3), p. 325-339.

Pal, S., Lojen, G., Hudak, R., Rajtukova, V., Brajlih, T., Kokol, V., Drstvenšek, I., 2020. As-fabricated surface morphologies of Ti-6Al-4V samples fabricated by different laser processing parameters in Selective Laser Melting. Additive Manufacturing 33, 101147.

Schleifenbaum, H., Meiners, W., Wissenbach, K., Hinke, C., 2010. Individualized production by means of high power Selective Laser Melting. CIRP Journal of manufacturing science and technology 2(3), p. 161-169.

Shi, W., Liu, Y., Shi, X., Hou, Y., Wang, P., Song, G., 2018. Beam diameter dependence of performance in thick-layer and high-power selective laser melting of Ti-6Al-4V. Materials 11(7), p. 1237.

Soylemez, E., 2020. High deposition rate approach of selective laser melting through defocused single bead experiments and thermal finite element analysis for Ti-6Al-4V. Additive Manufacturing 31, 100984.

Zhou, S., Su, Y., Gu, R., Wang, Z., Zhou, Y., Ma, Q., Yan, M., 2019. Impacts of defocusing amount and molten pool boundaries on mechanical properties and microstructure of selective laser melted AlSi10Mg. Materials 12(1), p. 73.